Crystal structure of tetrameric form of human lysyl-tRNA synthetase: Implications for multisynthetase complex formation

Min Guo*, Michael Ignatov†, Karin Musier-Forsyth†, Paul Schimmel*‡, and Xiang-Lei Yang*‡

*The Skaggs Institute for Chemical Biology and Department of Molecular Biology, The Scripps Research Institute, BCC-379, 10550 North Torrey Pines Road, La Jolla, CA 92037; and †Departments of Chemistry and Biochemistry, Ohio State University, Columbus, OH 43210

Contributed by Paul Schimmel, December 28, 2007 (sent for review December 7, 2007)

In mammals, many aminoacyl-tRNA synthetases are bound together in a multisynthetase complex (MSC) as a reservoir of procytokines and regulation molecules for functions beyond aminoacylation. The α_2 homodimeric lysyl-tRNA synthetase (LysRS) is tightly bound in the MSC and, under specific conditions, is secreted to trigger a proinflammatory response. Results by others suggest that α_2 LysRS is tightly bound into the core of the MSC with homodimeric β_2 p38, a scaffolding protein that itself is multifunctional. Not understood is how the two dimeric proteins combine to make a presumptive $\alpha_2\beta_2$ heterotetramer and, in particular, the location of the surfaces on LysRS that would accommodate the p38 interactions. Here we present a 2.3-Å crystal structure of a tetrameric form of human LysRS. The relatively loose (as seen in solution) tetramer interface is assembled from two eukaryote-specific sequences, one in the catalytic- and another in the anticodon-binding domain. This same interface is predicted to provide unique determinants for interaction with p38. The analyses suggest how the core of the MSC is assembled and, more generally, that interactions and functions of synthetases can be built and regulated through dynamic protein–protein interfaces. These interfaces are created from small adaptations to what is otherwise a highly conserved (through evolution) polypeptide sequence.

AIMP2 | aminoacyl-tRNA synthetase | p38

In higher eukaryotic cells, aminoacyl-tRNA synthetases (AARSs) are organized into a high molecular mass multisynthetase complex (MSC) (1), where at least nine AARSs and three accessory proteins are bound together (2). This complex is not only viable for highly organized protein synthesis (aminoacylation function) (3) but is also thought to serve as a reservoir of regulation molecules for functions beyond aminoacylation. For example, the unusual glutamyl-prolyl-tRNA synthetase (EPRS) in the MSC is released by stimulation with IFN-γ, which promotes phosphorylation of the WHEP domain in EPRS that, in turn, causes its release from the MSC (4). Once released, the phosphorylated EPRS is a component of a translation complex that directs gene-specific silencing of translation (4). As another example, when released from the MSC, human glutaminyl-tRNA synthetase specifically interacts with the apoptosis signal-regulating kinase 1 (ASK1) and inhibits ASK1-mediated apoptosis by inhibiting its kinase activity (5). Another component of the complex, lysyl-tRNA synthetase (LysRS), was recently shown to be secreted and to trigger a proinflammatory response (6). In addition, all three accessory proteins in the MSC, p43, p38, and p18 (also known as AIMP1, AIMP2, and AIMP3), have also been shown to have cytokine activities or to participate in different cell regulatory events (7, 8). The work presented here was motivated by the desire to understand better the structural basis for assembly of the MSC and how this assembly could be regulated in a way that expanded the functions of tRNA synthetases.

The functional importance of organization into a complex was suggested because the MSC *per se* was shown to be essential for normal development in the mouse (9). To regulate release of individual components requires that the MSC should be built up by diverse protein–protein interactions, ranging from stable to transient contacts. Indeed, various extra eukaryote-specific domains or extensions of AARSs have evolved to help form the MSC. For instance, the N-terminal coiled-coil appended domain of ArgRS is critical for interaction with p43 (10), and the N-terminal GST domain of MetRS possibly interacts with the GST domain of p18 (11, 12). However, formation of the MSC involves more than the domains added to these ancient enzymes. Mammalian LysRS is a component of the MSC that specifically interacts with the auxiliary factor p38 (11, 13). However, although a ≈70-aa extension was found to be unique to human LysRS, this lysine-rich extension does not contribute to the strong interaction with p38. Instead, the conserved canonical domains of human LysRS forms the p38-binding site(s) (11). Similarly, AspRS and GlnRS, with their eukaryotic-specific N-terminal extensions removed, were still associated with the complex (11, 14). These findings imply alternative ways of forming interactions between these ancient enzymes to endow them with the capacity for expanded functions. How these protein–protein interfaces are formed from ancient enzyme scaffolds is undefined and of particular interest.

The strong interaction of LysRS with p38, which forms the core of the MSC, and the observation that LysRS can be secreted as a signaling molecule intrigued us to understand the structural features that might explain the dynamics of LysRS, both in the complex and outside of the complex as a free protein. For this purpose, we carried out crystallization of human LysRS and determined its 3D structure. The crystals revealed an unusual $(\alpha_2)_2$ tetramer, a structure not seen with any of the other α_2 class II tRNA synthetases. More analysis showed that the interface for the α_2–α_2 interactions is most likely also used for interactions with p38 at the core of the MSC. That is, the tetramer interface, when exposed in the α_2 dimer, is well designed to interact with p38, and in a way that does not disturb the aminoacylation function of LysRS. The dynamic nature and design of this interface suggest a paradigm for how higher eukaryote tRNA synthetases can be mobilized to form different interactions and, thereby, adopt expanded functions.

Author contributions: M.G., M.I., K.M.-F., P.S., and X.-L.Y. designed research; M.G. and M.I. performed research; M.G., M.I., K.M.-F., P.S., and X.-L.Y. analyzed data; and M.G., P.S., and X.-L.Y. wrote the paper.

The authors declare no conflict of interest.

Data deposition: The atomic coordinates have been deposited into the Protein Data Bank, www.pdb.org (PDB ID code 3BJU).

‡To whom correspondence may be addressed. E-mail: schimmel@scripps.edu or xlyang@scripps.edu.

This article contains supporting information online at www.pnas.org/cgi/content/full/0712072105/DC1.

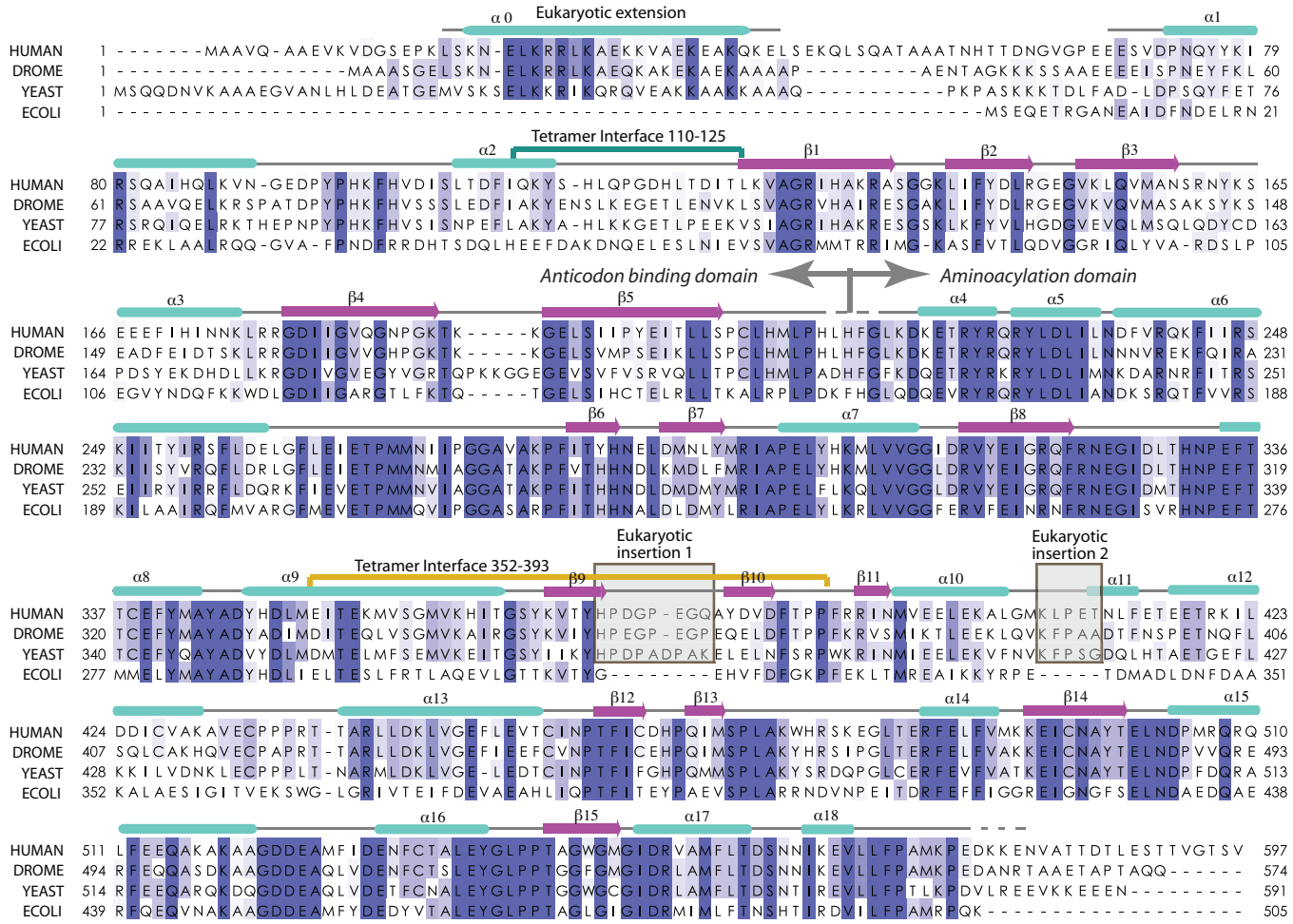

Fig. 1. Sequence alignment of class II LysRS from *Homo sapiens*, *Drosophila melanogaster*, *Saccharomyces cerevisiae*, and *E. coli* (LysU). The secondary structure elements derived from the crystal structure of human $LysRS_{70-584}$ are placed on top of the alignment. The missing N-terminal eukaryotic extension is predicted to contain a long α-helix, designated as $\alpha 0$.

Results

General Features of LysRSs in Evolution. There are two classes of tRNA synthetases, classes I and II, that are distinguished by the architectures of their active-site catalytic cores. Like most LysRSs, the human enzyme falls into class II. Regardless of the class, all tRNA synthetases are organized into a modular arrangement of functional domains along the sequence. In most instances, for both classes, the catalytic domain (containing the site for amino acid activation and docking of the 3′-end of the tRNA for aminoacylation) is located in the N-terminal part of the sequence. This N-terminal catalytic domain is the historical tRNA synthetase that arose early in evolution. It was present in the last common ancestor at the root of the tree of life that split into the three great kingdoms. Later, additional domains were fused to the catalytic domain, on its C-terminal side. The most common C-terminal domain evolved to interact with the anticodon triplets of the genetic code. Before addition of the C-terminal domain, the specificity of aminoacylation is believed to have been mainly generated from acceptor stem determinants in the early tRNAs and remain important determinants for tRNA specificity in many modern tRNAs (15).

In contrast to most tRNA synthetases, the class II LysRS (and the closely related AspRS and AsnRS) have a modular arrangement of functional domains that is reversed; that is, the catalytic domain is at the C-terminal end of the polypeptide, whereas the anticodon-binding site is encoded by the N-terminal part of the of the protein (16). In addition, the class II LysRS is one of the most conserved AARSs. Specifically, the sequence identity between human and *Escherichia coli* enzymes is 50% for the C-terminal aminoacylation domain and 26% for the N-terminal anticodon-binding domain (Fig. 1). This strong conservation of sequence is of particular interest, because the determinants that provide for novel interactions and expanded functions must be encoded within rather limited variations of sequence.

Tetrameric Crystal Structure of Human LysRS. Like other eukaryote LysRSs, human LysRS contains an N-terminal extension of its polypeptide sequence (Fig. 1). Truncation of the N-terminal extension decreased the catalytic efficiency only by threefold as a result of the reduced affinity for $tRNA^{Lys}$ and had no effect on the interaction with p38 (10, 17, 18). Both the full-length LysRS (M1-V597) and truncation (S70-T584) that removed the eukaryote-specific extension were expressed, purified, and attempted for crystallization. Only the truncated form was crystallized in the presence of ATP and L-lysine, and the crystals diffracted to 2.1-Å resolution with the space group of $P3_2$ [supporting information (SI) Table 1].

The structure was solved by molecular replacement by using a crystal structure of *E. coli* LysRS [LysU, Protein Data Bank (PDB) ID code 1E24] as the search model and was refined by using high-quality data up to 2.3-Å resolution. Four molecules of human LysRS with closely similar structures were found in the

asymmetric unit (maximum rmsd of 0.46 Å for 502 Cα atoms). The structure of each molecule harbors the N-terminal OB-fold anticodon-binding domain (S70-P214) that is specific to LysRS, AspRS, and AsnRS, and a C-terminal catalytic domain (L220-K574; the last 10 residues are disordered in the structure). This catalytic domain has the three motifs (motifs 1, 2, and 3) that are characteristic of class II enzymes and are part of a seven-stranded β-sheet with flanking α-helices (Fig. 2*A*). Each LysRS molecule contains bound L-lysine, ATP, and three calcium ions.

The structure of human LysRS closely resembles those of the two similar *E. coli* LysRSs, LysU (rmsd of 1.5 Å for 472 C_α atoms) and LysS (rmsd of 1.6 Å for 474 C_α atoms) (19, 20). Fig. 2*A* shows the structural comparison of human LysRS (green) and LysU (gray), with their catalytic domains superimposed. The most prominent difference between the two structures is the orientation of the anticodon-binding domain relative to their catalytic domain. A 5° rotation was observed, suggesting that the linkage between the two domains is flexible and, indeed, residues in the linker region were disordered for both human and *E. coli* LysRSs (Fig. 2*A*).

The four molecules of LysRS in the asymmetric unit form an unexpected $\alpha_2.\alpha_2$ tetramer, accounting for a calculated mass of ≈270 kDa. Interestingly, this tetramer is probably functional for aminoacylation, because docking of tRNA molecules to the tetrameric LysRS seems not to cause steric clash (see below).

Two of the four molecules in the asymmetric unit (referred to as LysRS-*a* and LysRS-*b*) form a virtually symmetric dimer (LysRS-*ab*) through the canonical class II AARS dimer interface that involves the characteristic motif 1. Similarly, the other two molecules (LysRS-*c* and LysRS-*d*) form the second dimer (LysRS-*cd*, Fig. 2*B*). The two dimers are almost identical to each other (rmsd of 0.17 Å for all 1,004 Cα atoms). Interestingly, although a symmetric surface of the two dimers was used, the dimer:dimer interaction was not symmetrical. The two dimers interact with each other only on one side (the bottom side of Fig. 2*B*) and not on the other side (the top side). In particular, subunit LysRS-*b* and subunit LysRS-*d* from each dimer directly contact each other to form the "on" interacting tetramer interface (Fig. 2*C*). In contrast, the other subunits, LysRS-*a* and LysRS-*c*, from each dimer have a ≈5-Å gap and form the "off" interacting tetramer interface (Fig. 2*D*). We surmise that this tetramer is an intermediate state of a loose tetramer that was captured in the crystal packing.

Confirmation of the Loose Tetramer in Solution. Because of the observation of the tetramer formation in the crystal structure, we wondered whether an α_4 tetramer form of the normally α_2 LysRS could be observed in solution. We imagined that a dimer–tetramer equilibrium could be shifted, under the crystallization conditions of high concentrations of LysRS, toward creating a major population of tetrameric species (through α_2–α_2 contacts) that was preferentially packed into the crystal. In the crystal structure, the tetramer contact is formed on only one side and has a gap on the other side (Fig. 2 *C* and *D*), suggesting that the interaction is weak and probably transient.

To characterize the putative tetramer interaction, we labeled full-length LysRS nonspecifically at 1:1 stoichiometry with Alexa488 and measured the concentration dependence of the fluorescence anisotropy and the fluorescence quantum yield (FQY). As the concentration of LysRS is raised, a sharp decrease in anisotropy is observed, consistent with a change in the shape and rotational dynamics of the protein (data not shown). Strikingly, the FQY shows a clear biphasic change, with a sharply diminished FQY at the initial part of the concentration dependence, followed by an increase at the higher concentrations (Fig. 3*A*). This behavior is consistent with the occurrence of two coupled equilibria, one consisting of a monomer–dimer and the other of a dimer–tetramer equilibrium. These two transitions

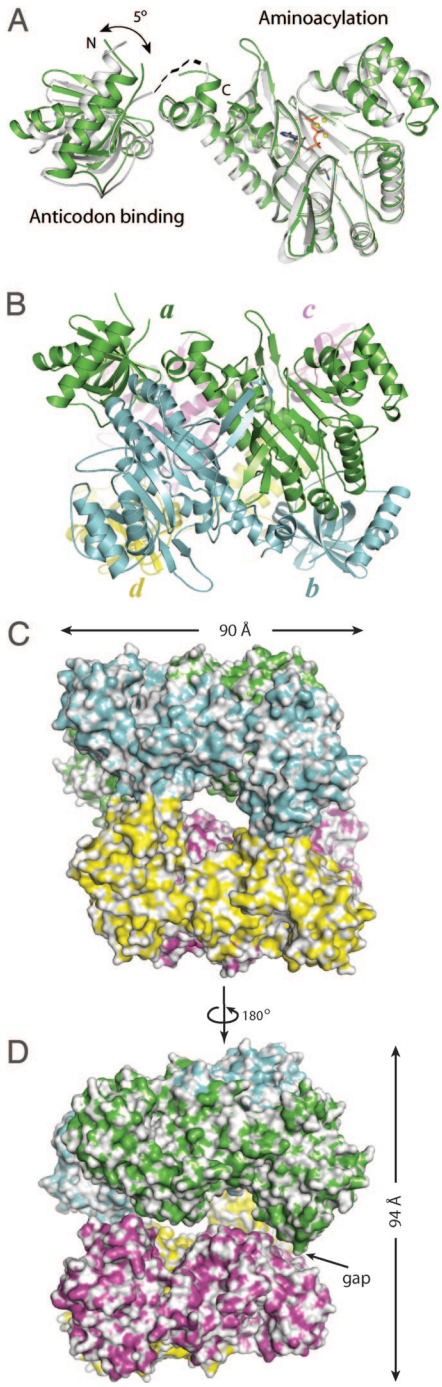

Fig. 2. The overall structural features of the human LysRS tetramer. (*A*) Superimposition of the catalytic domain in human LysRS (green) and with that of *E. coli* LysU (white). The bound ATP, L-lysine, calcium ions are also shown. (*B*) The asymmetric unit containing four LysRS molecules shown in different colors. The four molecules form two canonical dimers of LysRS (LysRS-*ab* and LysRS-*cd*). (*C* and *D*) Bottom and top views of the dimer:dimer interface, showing that the dimer:dimer contacts are asymmetric and formed only on one side but not on the other side of the tetramer.

have K_ds of 2 nM and 280 nM, respectively. These results encouraged the implementation of other experiments to further establish the loose dimer–tetramer equilibrium.

For this purpose, we used gel-filtration chromatography, with a loading concentration of LysRS (1.7 μM), well above the estimated K_d for the tetramer–dimer equilibrium. These data

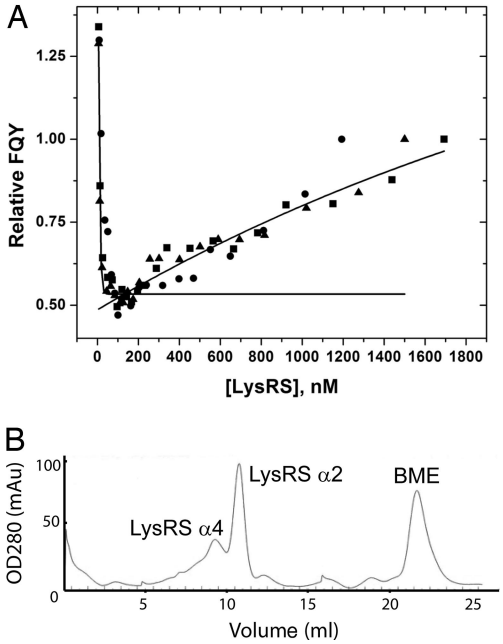

Fig. 3. Confirmation of the tetramer form of human LysRS in solution. (*A*) Fluorescence quantum yield titration. Two titration curves were fit with only low concentrations data (dimer formation) or only high concentrations data (tetramer formation) from triplicate datasets. (*B*) Superdex-200 gel-filtration profile of human LysRS loading at 1.7-μM concentration.

show the presence of two species, one at a molecular mass of ≈120 kDa and the other, a lesser peak, at ≈240 kDa (Fig. 3*B*). These results show clearly a dynamic dimer–tetramer oligomerization for LysRS.

Eukaryote-Specific Sequences used for LysRS Tetramer Assembly. In addition to the difference in the orientations of the anticodon recognition domains, a close comparison of the structure of human LysRS with that of *E. coli* LysU showed predominant differences at the tetramer interface (Fig. 4). The interface (between LysRS-*b* and LysRS-*d*) consists of two nearly symmetric binding sites, and each site involves interactions between an area including the α9-β9-loop-β10-loop from the C-terminal catalytic domain of LysRS-*b* (E352-R393) and a loop in between α2 and β1 from the anticodon-binding domain of LysRS-*d* (Q110-T125), and vice versa (Figs. 1 and 4*A*). Except for two specific interactions, the others are mainly through van der Waals contacts. One specific interaction is an H-bond formed between the main chain carboxyl group of P389 that adopts an unusual *cis* conformation and the carboxylate side chain of D123. The other is a salt bridge between K370 and D119 (Fig. 4*A*).

Interestingly, the tetramer interface is highly specific to eukaryotic LysRSs. One of the two eukaryote-specific insertions (H374-Q381) is embedded in the tetramer interface from the side of the catalytic domain (Fig. 1). *E. coli* LysRS lacks this insertion, which forms a long loop between β9 and β10 in human LysRS (Fig. 4*B*). Furthermore, the side of the anticodon-binding domain of the interface consists of residues with neither sequence nor structural homology to other LysRSs from lower organisms like *E. coli* (Figs. 1 and 4*B*). The idea of the tetramer interface being specific for human LysRS is reinforced when the structure is compared with that of the related AspRS (21) (Fig. 4*B*). Thus, the tetramer interface described here appears to be a hotspot for variations during evolution, including variations that can build a new protein–protein interface.

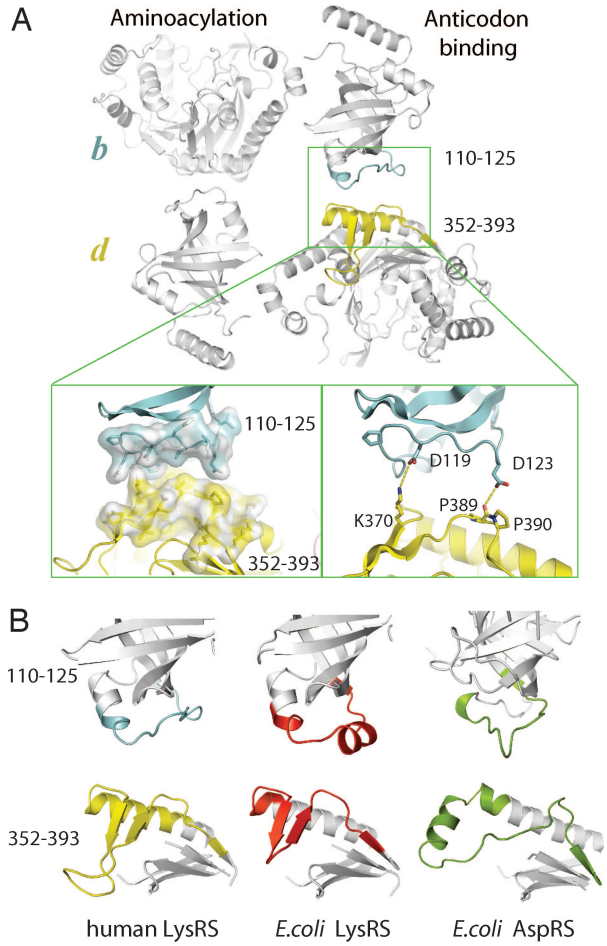

Fig. 4. The eukaryote-specific tetramer interface. (*A*) The *on*-interacting contacts of the tetramer interface between LysRS-*b* and -*d* with complementary van der Waals surfaces and specific interactions. (*B*) The tetramer interface regions are structurally distinct among human LysRS, *E. coli* LysRS, and AspRS. These *E. coli* enzymes are not known to make a tetramer interface.

Prediction of Tetramer Interface of LysRS for p38 Interaction. As shown by others (10), homodimeric α_2 LysRS binds to homodimeric β_2 p38 in a 1:1 ratio *in vitro*. Two molecules each of LysRS and p38 are bound in the MSC (13, 22). However, it is unclear how the two dimeric proteins interact with each other to make an $\alpha_2\beta_2$ heterotetramer, and, in particular, the location of the surfaces on LysRS that can accommodate the p38 interactions. For both human and *E. coli* LysRS, the α_2 dimer is required for charging $tRNA^{Lys}$ (23, 24). Given that LysRS within the MSC is fully functional for aminoacylation (22, 25), it is most likely that the α_2 form of LysRS interacts with the dimeric p38 in the MSC. With this in mind, we built a working model of the LysRS–tRNA complex and examined the remaining accessible surface for interactions with p38.

By superimposing the catalytic domain of human LysRS with that of *E. coli* AspRS in the AspRS-$tRNA^{Asp}$ complex (PDB ID code 1ASY), two tRNA molecules were docked onto the human LysRS dimer (Fig. 5*A*) on the side opposite to that of the tetramer interface (Fig. 5*B*). No steric clash occurred between either the dimeric or the tetrameric LysRS and the docked tRNA molecules. Because p38 binding did not affect aminoacylation activity (10, 22), we surmise that p38 does not compete with tRNA for binding to LysRS. In addition, the C-terminal region (452–597), including part of the motif 3, is disposable for p38 binding (26). These constraints enabled us to make a surface (on

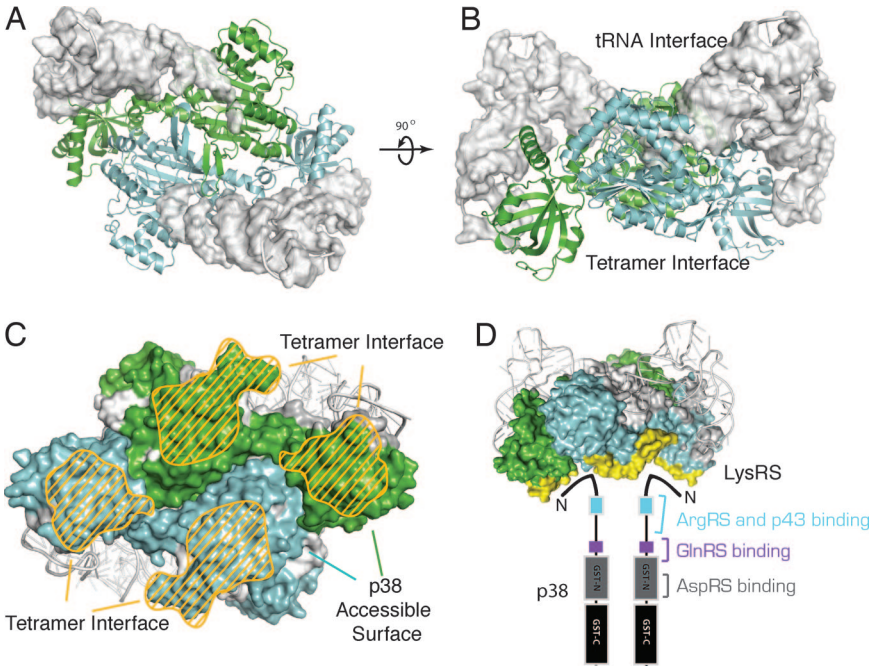

Fig. 5. The modeling of human LysRS complexed with tRNA and p38. (*A* and *B*) Top and side views of the dimeric LysRS-tRNA complex model. (*C*) Overlapping between the tetramer interface and the accessible surface for p38 on the LysRS dimer. The tRNA-binding surface, motifs 2–3 and C-terminal residues 452–597, which are not likely to be involved with p38 binding, are colored in gray. (*D*) The schematic model of the $\alpha_2\beta_2$ LysRS:p38 complex with tRNA bound to LysRS. The predicted interaction sites for LysRS, ArgRS, p43, GlnRS, and AspRS on p38 are taken from ref. 11.

the dimeric LysRS structure) that was accessible to p38. This surface is shown in Fig. 5*C* in green and blue for LysRS-*a* and -*b*, respectively.

Remarkably, the p38-accessible surface greatly overlapped with the tetramer interface (Fig. 5*C*). The four areas of the eukaryote-specific tetramer interface are well positioned for the potential p38 binding. These positions are symmetrical through a twofold axis that lies along the dimer interface of LysRS. Each monomer of p38 is thought to have a single binding site for one subunit of LysRS and, at the same time, the stable LysRS:p38 association needs the dimeric form of p38 (11). Therefore, the binding interface between LysRS and p38 would also be symmetrical, along the same twofold axis of the LysRS dimer interface. A schematic model of the $\alpha_2\beta_2$ LysRS:p38 complex is shown in Fig. 5*D*. As the core of the MSC, p38 contains binding sites for LysRS, AspRS, GlnRS, ArgRS, and p43 (11). In particular, the LysRS-binding site was found to be at the N-terminal region of p38 (10).

In conclusion, we view the binding of the dimeric β_2 p38 to α_2 LysRS to be competitive with the association of LysRS dimers to form an $(\alpha_2)_2$ tetramer. With this scenario, the same interface used for the LysRS dimer:dimer interaction outside the MSC is reused for associating with p38 in the MSC.

Discussion

Homotetrameric forms of the normally homodimeric class II tRNA synthetases are scare. As an example, the α_4 AlaRS is unique to *E. coli* and is not seen in other organisms. However, the *E. coli* AlaRS tetramer is far more stable than the human LysRS tetramer. The α_4 AlaRS binds to a DNA palindrome in the promoter of the gene *alaS* and thereby regulates expression of AlaRS, in an alanine-dependent way (27). Suberimidate cross-linking experiments established that the AlaRS α_4 tetramer, like human LysRS, is a dimer of dimers (28). A direct biological role for the human LysRS tetramer is not known. But regardless of the biological role (if any) of the tetramer, that it can form at concentrations in the low micromolar range (Fig. 3*B*) suggests, in principle, it is present *in vivo*, where tRNA synthetase concentrations are on the order of micromolar.

Even without a direct biological role, our structural work suggests that the α_2–α_2 interaction is competitive with the interaction of LysRS with p38, to form the core of the multisynthetase complex. Thus, the dimer–tetramer equilibrium may have a role in regulating the assembly of the complex. In addition, in humans, LysRS interacts with mutant forms of Cu, Zn superoxide dismutase (SOD1) (29), HIV-1 Gag protein (23), and a cellular protein TIP-15 (30). In general, we cannot determine whether these additional interactions would overlap with the dimer–dimer interface and the proposed interaction surface for p38 and thereby introduce another pathway that could affect the assembly of the multisynthetase complex. Because the C terminus of LysRS matches the consensus motif for the PDZ binding domain, the PDZ-containing TIP-15 may bind the C-terminal end of LysRS. Given that the C terminus of LysRS is dispensable for p38 binding (26), association of TIP-15 with LysRS may not interfere with p38 binding. Finally, Gag was shown to bind to the dimer interface of LysRS and to disrupt the LysRS dimer by forming a LysRS-Gag heterodimer (23). Disruption of the dimer most likely would also affect interaction with p38.

If validated by further analysis and experiments, the appearance in evolution of eukaryote-specific regions that enable functional expansion (interaction with p38 for MSC assembly) of LysRS is striking. In this instance, the sequences enable interaction of LysRS with p38 in a way that does not disturb the essential aminoacylation function. For human TrpRS, functional expansion (for potent angiostatic activity) required not only the acquisition of sequences in evolution but also a structural adaptation of the active-site region that enabled the enzyme to maintain its aminoacylation function, while also being able to regulate the activation of its cytokine function (31). In contrast to TrpRS, no active-site adaptation was needed for the p38

interaction, probably because the interaction itself can be regulated in a simple way (competition with the dimer–tetramer equilibrium of LysRS). Whether the p38-LysRS complex has an additional activity emanating, for example, from the interface of the two proteins, will also require further investigation.

Methods

Protein Preparation. Full-length LysRS and truncation $LysRS_{70-584}$ were expressed in the bacterial strain BL21 (DE3) CodonPlus using the vectors pET20b (Novagen). Both proteins contained a C-terminal 6 ×His tag and were purified to homogeneity by Ni-NTA affinity column (Qiagen) and a Q high-performance column (GE Healthcare).

Crystallization, Data Collection, and Structure Determination. Crystallization was done by the micrositting drop-vapor diffusion method. Protein solution of $LysRS_{70-584}$ was preincubated with 5 mM L-lysine and 5 mM ATP for 10 min at 22°C. A drop was prepared by mixing 0.1 μl of protein solution with 0.1 μl of precipitant solution, containing 16% PEG8K, 18% glycerol, 80 mM Na cacodylate (pH 6.05), and 0.16 M $Ca(OAc)_2$ and was equilibrated against 70 μl of precipitant solution. Crystals were collected after incubation at 4°C for 7 days and were flash-frozen at 100 K for data collection.

The dataset was obtained from beamline 23-ID at the Advanced Photo Source (Argonne, IL) and was processed with HKL2000 (32). Iterative model building and refinement were performed by using Coot (33) and Refmac5 (34). Data collection and refinement statistics are given in SI Table 1.

Gel Filtration Chromatography. A volume of 500 μl of purified full-length LysRS was applied to Superdex 200 chromatography column (GE Healthcare, 10/300 GL) in a buffer containing 25 mM Hepes, pH 7.5, 150 mM NaCl, and 5 mM 2-mercaptoethanol, and the column was calibrated by standard proteins.

Labeling of Human LysRS with Alexa488. Human LysRS was diluted into 50 mM sodium phosphate buffer, pH 8.5, to a final concentration of 5 μM (measured by absorption at 280 nm using extinction coefficient of 44,280 $M^{-1}\cdot cm^{-1}$) and Alexa488-tetrafluorophenyl ester (Invitrogen) was dissolved in DMSO and added to a final concentration of 5 μM (determined by measuring the absorption at 495 nm using ε_{495} = 71,000 $M^{-1}\cdot cm^{-1}$). The labeling reaction proceeded at room temperature for 30 min, and the sample was buffer exchanged (12 times) and concentrated by using Amicon Ultra - 4 spin concentrators with molecular weight cutoff of 10,000 Da (Millipore). The degree of labeling was determined to be 0.93:1 dye to protein by measuring the absorption at 495 and 280 nm in a 1-cm cuvette using the following equation:

$$A^{495} \times \varepsilon^{280}_{\text{Protein}}/((A^{280} - 0.11 \times A^{495}) \times \varepsilon^{495}_{\text{Alexa}}).$$

Fluorescence Quantum Yield Measurements. Full fluorescence spectra of Alexa488-labeled human LysRS were recorded by using a Cary Eclipse fluorometer (Varian) with the excitation monochromator set to 460 nm and emission scanned from 475–650 nm. Fluorescence spectra were measured in triplicate as a function of increasing protein concentration. The integrated spectra were normalized to the highest protein concentration. The curves were biphasic, and the two parts were independently fitted to a single-exponential function to obtain the midpoints of the titration. Assuming a 1:1 binding of monomers to form a dimer and 1:1 binding of dimers to form a tetramer, it can be deduced that at the measured midpoints, the K_d is equal to one-third of the total protein concentration. Multiple datasets were globally analyzed to produce a more robust estimate of the dissociation constants.

ACKNOWLEDGMENTS. We thank Prof. David Yang (Georgetown University, Washington, DC) and Prof. Murray Deutscher (University of Miami Miller School of Medicine, Miami) for comments on the manuscript, Dr. Kumar Singh Saikatendu for help on the data collection at the Advanced Photon Source, and Dr. My Vo for helpful discussions. This work was supported by Grants GM15539 (to P.S.) and AI054145 (to K.M.-F) from the National Institutes of Health and by a grant from the National Foundation for Cancer Research.

1. Lee SW, Cho BH, Park SG, Kim S (2004) Aminoacyl-tRNA synthetase complexes: beyond translation. *J Cell Sci* 117:3725–3734.
2. Kerjan P, Cerini C, Semeriva M, Mirande M (1994) The multienzyme complex containing nine aminoacyl-tRNA synthetases is ubiquitous from Drosophila to mammals. *Biochim Biophys Acta* 1199:293–297.
3. Kyriacou SV, Deutscher MP (2008) An important role for the multienzyme aminoacyl-tRNA synthetase complex in mammalian translation and cell growth. *Mol Cell*, in press.
4. Sampath P, *et al.* (2004) Noncanonical function of glutamyl-prolyl-tRNA synthetase: gene-specific silencing of translation, *Cell* 119:195–208.
5. Ko YG, *et al*. (2001) Glutamine-dependent antiapoptotic interaction of human glutaminyl-tRNA synthetase with apoptosis signal-regulating kinase 1. *J Biol Chem* 276:6030–6036.
6. Park SG, *et al*. (2005) Human lysyl-tRNA synthetase is secreted to trigger proinflammatory response. *Proc Natl Acad Sci USA* 102:6356–6361.
7. Park BJ, *et al*. (2005) The haploinsufficient tumor suppressor p18 upregulates p53 via interactions with ATM/ATR. *Cell* 120:209–221.
8. Park H, Park SG, Kim J, Ko YG, Kim S (2002) Signaling pathways for TNF production induced by human aminoacyl-tRNA synthetase-associating factor, p43. *Cytokine* 20:148–153.
9. Kim MJ, *et al*. (2003) Downregulation of FUSE-binding protein and c-myc by tRNA synthetase cofactor p38 is required for lung cell differentiation. *Nat Genet* 34:330–336.
10. Robinson JC, Kerjan P, Mirande M (2000) Macromolecular assemblage of aminoacyl-tRNA synthetases: quantitative analysis of protein-protein interactions and mechanism of complex assembly. *J Mol Biol* 304:983–994.
11. Quevillon S, Robinson JC, Berthonneau E, Siatecka M, Mirande M (1999) Macromolecular assemblage of aminoacyl-tRNA synthetases: identification of protein-protein interactions and characterization of a core protein. *J Mol Biol* 285:183–195.
12. Simader H, Hothorn M, Kohler C, Basquin J, Simos G, Suck D (2006) Structural basis of yeast aminoacyl-tRNA synthetase complex formation revealed by crystal structures of two binary sub-complexes. *Nucleic Acids Res* 34:3968–3979.
13. Johnson DL, Yang DC (1981) Stoichiometry and composition of an aminoacyl-tRNA synthetase complex from rat liver. *Proc Natl Acad Sci USA* 78:4059–4062.
14. Kim T, *et al*. (2000) Catalytic peptide of human glutaminyl-tRNA synthetase is essential for its assembly to the aminoacyl-tRNA synthetase complex. *J Biol Chem* 275:21768–21772.
15. Schimmel P, Ribas de Pouplana L (1995) Transfer RNA: from minihelix to genetic code. *Cell* 81:983–986.
16. Cusack S (1995) Eleven down and nine to go. *Nat Struct Biol* 2:824–831.
17. Francin M, Kaminska M, Kerjan P, Mirande M (2002) The N-terminal domain of mammalian Lysyl-tRNA synthetase is a functional tRNA-binding domain. *J Biol Chem* 277:1762–1769.
18. Guzzo CM, Yang DC (2008) Lysyl-tRNA synthetase interacts with EF1α, aspartyl-tRNA synthetase and p38 in vitro. *Biochem Biophys Res Commun*, 365:718–723.
19. Onesti S, *et al*. (2000) Structural studies of lysyl-tRNA synthetase: conformational changes induced by substrate binding. *Biochemistry* 39:12853–12861.
20. Onesti S, Miller AD, Brick P (1995) The crystal structure of the lysyl-tRNA synthetase (LysU) from Escherichia coli. *Structure (London)* 3:163–176.
21. Ruff M, *et al*. (1991) Class II aminoacyl transfer RNA synthetases: crystal structure of yeast aspartyl-tRNA synthetase complexed with tRNA(Asp). *Science* 252:1682–1689.
22. Mirande M, Cirakoglu B, Waller JP (1983) Seven mammalian aminoacyl-tRNA synthetases associated within the same complex are functionally independent. *Eur J Biochem* 131:163–170.
23. Kovaleski BJ, *et al*. (2006) In vitro characterization of the interaction between HIV-1 Gag and human lysyl-tRNA synthetase. *J Biol Chem* 281:19449–19456.
24. Commans S, Blanquet S, Plateau P (1995) A single substitution in the motif 1 of Escherichia coli Lysyl-tRNA synthetase induces cooperativity. *Biochemistry* 34:8180–8189.
25. Dang CV, Ferguson B, Burke DJ, Garcia V, Yang DC (1985) Interactions of aminoacyl-tRNA synthetases in high-molecular-weight multienzyme complexes from rat liver. *Biochim Biophys Acta* 829:319–326.
26. Halwani R, Cen S, Javanbakht H, Saadatmand J, Kim S, Shiba K, Kleiman L (2004) Cellular distribution of Lysyl-tRNA synthetase and its interaction with Gag during human immunodeficiency virus type 1 assembly. *J Virol* 78:7553–7564.
27. Putney SD, Schimmel P (1981) An aminoacyl tRNA synthetase binds to a specific DNA sequence and regulates its gene transcription. *Nature* 291:632–635.
28. Putney SD, Sauer RT, Schimmel PR (1981) Purification and properties of alanine tRNA synthetase from Escherichia coli: A tetramer of identical subunits. *J Biol Chem* 256:198–204.
29. Kunst CB, Mezey E, Brownstein MJ, Patterson D (1997) Mutations in SOD1 associated with amyotrophic lateral sclerosis cause novel protein interactions. *Nat Genet* 15:91–94.
30. Fabre S, Reynaud C, Jalinot P (2000) Identification of functional PDZ domain binding sites in several human proteins. *Mol Biol Rep* 27:217–224.
31. Yang XL, *et al*. (2007) Functional and crystal structure analysis of active site adaptations of a potent anti-angiogenic human tRNA synthetase. *Structure (London)* 15:793–805.
32. Otwinowski Z, Minor W (1997) Processing of X-ray diffraction data collected in oscillation mode. *Methods Enzymol* 276:307–326.
33. Emsley P, Cowtan K (2004) Coot: model-building tools for molecular graphics. *Acta Crystallogr D* 60:2126–2132.
34. CCP4 (1994) The CCP4 suite: programs for protein crystallography. *Acta Crystallogr D* 50:760–763.